Topological characteristics of model gels

2010 J. Phys.: Condens. Matter 22 104109

(http://iopscience.iop.org/0953-8984/22/10/104109)

J. Phys.: Condens. Matter **22** (2010) 104109 (8pp) doi:10.1088/0953-8984/22/10/104109

Topological characteristics of model gels

Mark A Miller[1], Ronald Blaak[2] and Jean-Pierre Hansen[1]

[1] University Chemical Laboratory, Lensfield Road, Cambridge CB2 1EW, UK
[2] Institute for Theoretical Physics II: Soft Matter, Heinrich-Heine-Universität Düsseldorf, Universitätsstraße 1, D-40225 Düsseldorf, Germany

Received 4 October 2009, in final form 4 November 2009
Published 23 February 2010
Online at stacks.iop.org/JPhysCM/22/104109

Abstract
The Euler characteristic of an object is a topological invariant determined by the number of handles and holes that it contains. Here, we use the Euler characteristic to profile the topology of model three-dimensional gel-forming fluids as a function of increasing length scale. These profiles act as a 'topological fingerprint' of the structure, and can be interpreted in terms of three types of topological events. As model fluids we have considered a system of dipolar dumbbells, and suspensions of adhesive hard spheres with isotropic and patchy interactions in turn. The correlation between the percolation threshold and the length scale on which the Euler characteristic passes through zero is examined and found to be system-dependent. A scheme for the efficient calculation of the Euler characteristic with and without periodic boundary conditions is described.

(Some figures in this article are in colour only in the electronic version)

1. Introduction

Colloidal gels can be made from a wide array of different particles and by many different routes. However, their common and defining features include low density, disordered structure and some degree of dynamical arrest [1]. Gels therefore often take the form of a percolating network, in which chain-like structures are interlinked at junctions, and sizeable voids are encompassed.

One way to encourage the formation of such open structures with respect to more compact ones is through anisotropic or patchy interactions. An advantage of this route to gel formation is that limiting the coordination number of the particles decreases the critical temperature and density of the gas–liquid-like transition. This means that gelation can be studied reversibly, without the intervention of phase separation, to arbitrarily low densities [2]. A more general understanding of gels has been gained in recent years from studying idealized models with a combination of theoretical tools and computer simulation [3, 4].

Common structural measures like the radial distribution function and its Fourier transform, the static structure factor, naturally provide useful information about gel structure. However, these quantities are based on the direct distances between particles through space, and therefore do not always reveal whether or how a pair of particles are connected through the intervening structure. For gel-like networks, a clearer picture of this connectivity can be helpful, making a topological analysis desirable.

In this paper, we investigate the Euler characteristic (EC) as a tool for quantifying the topology of model gels as a function of length scale. In section 2, we specify the models and outline the simulations that were performed. The EC is then introduced and used to analyse the gels in section 3. The connection between the EC and the percolation threshold is investigated in section 4. We then provide a summary and some closing remarks in section 5. The appendix describes how the EC can be calculated efficiently and addresses issues related to periodic boundary conditions and structural data derived from experiments.

2. Models and simulations

2.1. Dipolar dumbbells

The first model studied is a fluid of soft dipolar dumbbells, introduced recently to explore network formation and dynamical arrest in a physical gel [5, 6]. Dipolar particles readily aggregate into chains [7], but chains of point dipolar spheres show only a weak tendency to form interconnecting junctions [8]. Extending the repulsive core into a dumbbell and at the same time separating the point dipole into discrete charges enhances network formation [5].

Our dumbbells consist of two interaction sites separated by a fixed distance d, each carrying a soft repulsive core and a

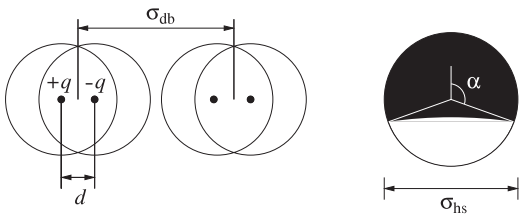

Figure 1. Schematic diagrams of the dipolar dumbbell model (left) and a patchy adhesive hard sphere (right). In the latter, the black region represents the adhesive patch and we have taken $\alpha = 101.54°$ such that the patch covers 60% of the surface. Two patchy spheres attract only if their point of contact lies within the black region of both spheres.

point charge—one of $+q$ and the other of $-q$ (figure 1). For two sites on different dumbbells separated by r, the repulsive interaction is c/r^{12} while the charge–charge interaction is the Coulomb energy $\pm q^2/4\pi\epsilon_0\epsilon' r$. Here, ϵ_0 and ϵ' are the permittivity of free space and the relative permittivity of the medium, respectively.

We define the reduced unit of length σ_{db} to be the separation of the dumbbell centres in the head-to-tail configuration of lowest pair energy. The natural unit of energy is then $u = \mu^2/4\pi\epsilon_0\epsilon'\sigma_{\mathrm{db}}^3$, where $\mu = qd$ is the dipole moment of a dumbbell. In terms of these definitions, we have set the repulsion coefficient at $c = 0.0208u\sigma_{\mathrm{db}}^{12}$ and the separation of sites at $d = 0.217\sigma_{\mathrm{db}}$. Reduced density and temperature are defined by $\rho^* = N\sigma_{\mathrm{db}}^3/V$ and $T^* = k_{\mathrm{B}}T/u$, respectively, where k_{B} is Boltzmann's constant and the simulation cell contains N particles in a volume V. We will take $\phi = \pi\rho^*/6$ as an estimate of the packing fraction.

Systems of $N = 1000$ dumbbells were simulated with the GROMACS package [9] using a Berendsen thermostat [10] and the standard Verlet leapfrog algorithm [11] for constant-temperature molecular dynamics, with cubic periodic boundary conditions and the particle-mesh Ewald method for the electrostatics [11]. Although Newtonian dynamics neglects both the Brownian motion of the particles and the hydrodynamic effect of the solvent in a colloidal suspension, the present work is concerned only with equilibrium structure, on which the details of the dynamics have no effect.

The gas–liquid-like critical point of soft dipolar dumbbells has very recently been calculated by Braun and Hentschke [12]. Our model is mapped onto equation (1) of their work by taking $d = 0.389$. Converting to our scheme of reduced units, the critical temperature is $T_{\mathrm{c}}^* = 0.18$ and the critical packing fraction lies at the very low value of $\phi_{\mathrm{c}} = 0.014$. Although we have studied a temperature range that includes significantly subcritical values, our packing fractions are relatively high (though still not dense by the standards of liquids) and we have not observed signatures of phase separation [5, 6].

2.2. Adhesive hard spheres

The structure of the dipolar dumbbell fluid is dominated by self-assembled chains, which lead to percolating networks at rather low packing fractions. As a contrasting example, we also study systems of adhesive hard spheres [13] (AHS), which are the archetypal model for suspensions of spherical colloidal particles with strong short-range attractive forces.

The AHS potential $U(r)$ is derived from a hard sphere with square well attraction by taking the limit where the well depth becomes infinite at the same time as its width becomes infinitesimal in such a way that the second virial coefficient remains finite [13]. The resulting potential is most concisely expressed in terms of the Boltzmann factor:

$$\mathrm{e}^{-U(r)/kT} = \Theta(r - \sigma_{\mathrm{hs}}) + \frac{\sigma_{\mathrm{hs}}}{12\tau}\delta(r - \sigma_{\mathrm{hs}}), \qquad (1)$$

where σ_{hs} is the diameter of the hard core and τ is an effective temperature or inverse stickiness, which replaces the thermodynamic temperature T. The Heaviside step function Θ sets the weight of any configuration with overlapping hard cores to zero, while the Dirac δ function accounts for the adhesive attraction at particle contact. The packing fraction is unambiguously defined by $\phi = N\pi\sigma_{\mathrm{hs}}^3/6V$.

The adhesive limit has the advantage that the integrated Boltzmann weights for a particle with one, two or three bonds can be calculated analytically. This means that a dedicated Monte Carlo algorithm can be devised, in which steps consist not of random displacements, but of the explicit making and breaking of up to three bonds at a time [14–16]. Highly coordinated states can be reached through a sequence of such steps. A detailed account of the simulation method can be found in [17].

The attraction described by equation (1) is isotropic. We have also examined a patchy version of the AHS model, in which the attractive interaction does not apply to the entire surface of the spheres. Instead, each particle has a circular patch that subtends an angle 2α at the centre of the sphere [18, 19] (figure 1). Two spheres may only adhere if the point of contact between them lies within the patch on both particles. If the contact lies outside one or both of the patches, the interaction is that of hard spheres. This modification of the AHS potential amounts to inserting an angular criterion in front of the δ function in equation (1) and is straightforward to incorporate into the Monte Carlo algorithm [19].

We have chosen a patch angle of $\alpha \approx 101.54°$, such that the fraction of the sphere surface covered by the patch is $S = \sin^2(\alpha/2) = 0.6$. Although more than half the surface remains adhesive, the structure of the fluid is disrupted by the geometric constraints that bonds must satisfy in order for the patches on adjacent spheres to align. The second virial coefficient of the patchy AHS model is [19] $B_2 = B_2^{\mathrm{hs}}(1 - S^2/4\tau)$, where B_2^{hs} is the hard sphere value. Hence, the isotropic AHS (equivalent to $S = 1$) and patchy AHS should be compared at values of the scaled effective temperature $\tau' = \tau/S^2$ to account for the trivial effect of removing some of the attraction in the patchy case.

3. Euler characteristic

In recent work the Euler characteristic χ has been used as a tool for structural analysis [6, 20] to complement more common

quantities like the radial distribution function, the structure factor and other correlation functions. The EC has been particularly informative in systems where the structure has prominent topological features such as loops or tunnels [21]. In three dimensions, the EC is related to one of the four scalar Minkowski functionals that describe a surface. These functionals are, respectively, the volume enclosed by the surface, the total surface area and both surface integrals of the mean and Gaussian curvature. If the latter is normalized by a factor 2π, we obtain the EC. Somewhat surprisingly, this quantity is an integer related to the number of objects, handles and holes in the surface. An alternative approach to calculating the EC is via a tessellation of the surface with convex polygons and application of Euler's result $\chi = V - E + F$, where V, E, and F denote the number of vertices, edges and faces, respectively, in the tessellated surface.

To analyse the structure of a collection of particles using the EC, it is necessary to associate a surface with any instantaneous configuration specified by the positions $\mathbf{r}_i$ ($i = 1, \ldots, N$) of the particles. Clearly there are many possible ways to introduce such a surface, but a particularly simple choice is obtained by using iso-surfaces of the function

$$\Phi(\mathbf{X}) = \min_i |\mathbf{X} - \mathbf{r}_i|, \tag{2}$$

where $\mathbf{X}$ is a point in the three-dimensional space occupied by the particles. The surface $\Phi(\mathbf{X}) = R$ is then formed by the joined surfaces of spheres with radius R centred at the positions of the particles. For this specific family of surfaces, the Euler characteristic $\chi(R)$ can be calculated efficiently.

Due to its discrete nature, the EC varies with R through a series of discontinuous jumps. These jumps occur when an 'event point' is incorporated into the surface, changing its topology. A given point in space that is nearest to only a single coordinate $\mathbf{r}_i$ cannot be an event point. This follows from the fact that the EC of a surface is invariant under continuous deformation of that surface, in particular a deformation in which part of a spherical surface is modified by increasing its radius. Hence, an event point must lie at equal distance from at least two particles with no other particles being closer. Consequently, all event points must lie on the boundary of the Voronoi cells defined by the particle coordinates.

For small values of R, the surface $\Phi(\mathbf{X}) = R$ is formed by N non-overlapping spheres. Since the EC of a single sphere is 2, the EC of the total surface is $\chi(R) = 2N$. By gradually increasing the radius of all spheres simultaneously, we can follow the development of the surface and, at specific values of R, observe changes in the topology of the surface that change the EC. In three dimensions one can distinguish three types of events that lead to a discontinuous topological change of the surface $\Phi(\mathbf{X}) = R$ and that hence change the EC:

(1) A two-particle event occurs when two spheres touch at $\mathbf{X}$. If the two partial surface areas were not connected before, the number of disjunct surfaces is decreased by one, otherwise an additional loop (handle) is formed in the surface. In either case the EC is decreased by 2. The event point itself lies halfway between the two particles involved and, since no particle lies closer (otherwise $\Phi(\mathbf{X}) < R$), it necessarily lies on the common face of the Voronoi cells of the two particles.

(2) A three-particle event takes place when a point $\mathbf{X}$ on the surface lies at an equal distance R from three particles that have mutual separations less than $2R$. In that case an existing loop in the surface is removed, increasing the EC by 2. Since no other particle is found nearer, the event point lies on an edge common to the three Voronoi cells of the particles involved. See figure 2 for illustrations of this type of event both on the length scale of individual particles and on that of larger loops in the structure.

(3) A four-particle event is found at a point $\mathbf{X}$ on the surface that is equidistant to four non-coplanar particles, each at distance R from $\mathbf{X}$ and which lies within the tetrahedron defined by the four particles' coordinates. This topological event removes a cavity (hole) that exists for $\Phi(\mathbf{X}) < R$, thus decreasing the EC by 2. Such an event point lies at a vertex common to the Voronoi cells of the four particles.

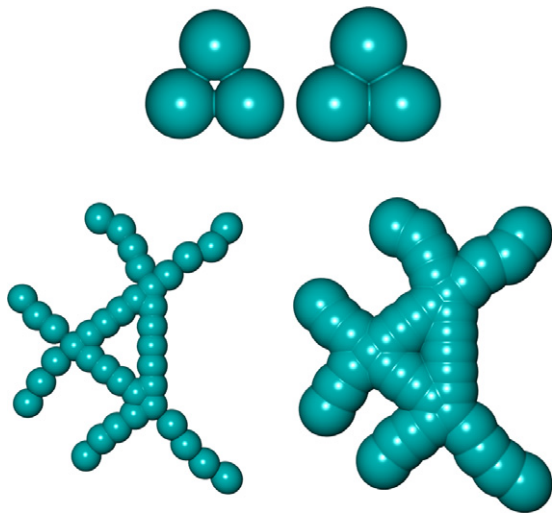

Figure 2. Closure of loops (handles) on two length scales as the diameter D grows: triplets of neighbouring particles (upper panels) and loops formed by branched chains (lower panels).

The effect that each of these events has on the EC can be checked by careful examination of a tessellation of the surface and counting the difference in the number of faces, edges and vertices caused by the event. It should be noted that, in certain specific geometries, three- and four-particle events can occur at points that are equidistant from more than three or four particles, respectively. For example, a three-particle event can take place on a Voronoi edge that is common to four, rather than to three, cells. However, it is not necessary to search for such cases specifically, since they are automatically detected when any three or four of the particles, respectively, are considered.

In order to compute the EC, we need to detect all possible events and evaluate the numbers $N_i(R)$ of i-particle events ($i = 2, 3, 4$) that take place at radii less than R. The cumulative nature of these functions can be exploited to enhance efficiency of the computation. The EC as a function of the sphere radius R follows from

$$\chi(R) = 2[N - N_2(R) + N_3(R) - N_4(R)]. \tag{3}$$

This function tracks the evolution of the system's topology as the length scale specified by R is varied. In order to facilitate comparison between different cases, we will in the remainder of this paper normalize the EC by dividing it by its value, $2N$, at small R. For sufficiently large R, a periodic system is completely engulfed by the merged spheres and none of the surface Φ remains. The normalized EC, $\kappa = \chi/2N$, will therefore start with a plateau at unity and converge to zero for large radii. In addition, we will use the diameter $D = 2R$, rather than the radius, to characterize the notional sphere centred on each particle. If we denote the contributions to the EC of the different types of events by $n_i(D) = N_i(R)/2N$, we obtain

$$\kappa(D) = 1 - n_2(D) + n_3(D) - n_4(D). \tag{4}$$

Figure 3(a) shows the Euler characteristic profile $\kappa(D)$, averaged over a trajectory, for the dipolar dumbbell fluid at a packing fraction of $\phi = 0.0745$ at a series of reduced temperatures T^* [6]. At high temperatures, the particles do not cluster and the structure of the fluid is close to that of an ideal gas. The EC profile therefore approaches a limiting form corresponding to randomly distributed points (see equation (5) in section 4). This profile simply scales with density as $\phi^{-1/3}$ along the D axis. As the fluid is cooled, small chain-like clusters appear, leading to a large number of two-particle events around $D = \sigma_{\mathrm{db}}$ and a steep drop in $\kappa(D)$. The EC profile continues to change as T^* is lowered through the percolation temperature 0.177 [5], and its first minimum shifts to smaller D as the majority of particles become incorporated into long chains. The percolation threshold marks the point where the chains of dipoles first become connected across the periodic boundary conditions. However, the structure evolves significantly as T^* is lowered still further, developing an increasingly sharp dip near $D = \sigma_{\mathrm{db}}$ as the chains begin to bundle. Segments of parallel chains lead to the formation and then closure of small tori of three neighbouring particles of the type illustrated at the top of figure 2. The sensitivity of the EC to these ongoing changes is one of its strengths as a structural measure.

In contrast, figure 3(b) shows the equivalent EC profiles for a modified version of the dumbbell model, where the distance d between the interaction sites has been contracted to one-fifth of the value given in section 2. The charges q have been increased by a factor of 5 to keep the dipole moment $\mu = qd$ unchanged. The fact that these more point-like dipoles in a more spherical core are less prone to network formation is evident from the EC profile. On cooling from a high temperature, the steep drop in $\kappa(D)$ arises as in the original dumbbell model, but this drop now terminates abruptly close to $\kappa = 0$. The zero in κ is the result of each particle in a chain having two neighbours, which leads to $N_2 = N$ two-particle events and $\chi = 0$ in equation (3). The EC only changes again when D becomes large enough to connect independent chains. Furthermore, the almost unchanging EC profile at the lowest few temperatures in figure 3(b) illustrates that the structure of the fluid of contracted dumbbells is much less responsive to T^* than that of the original dumbbell model.

To understand how the EC profile varies with diameter, it can be helpful to examine the contributions n_1, n_2 and

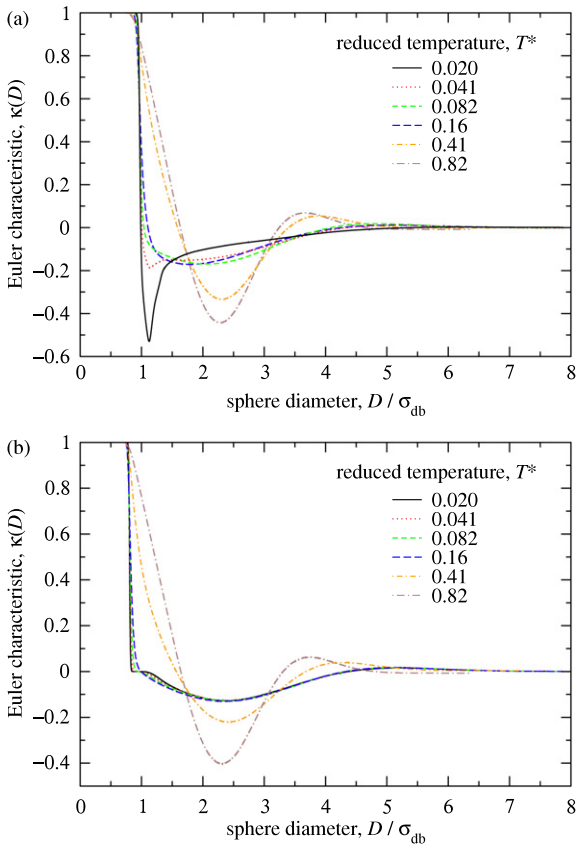

Figure 3. Euler characteristic profiles for dipolar dumbbells at packing fraction $\phi = 0.0745$ and a series of reduced temperatures, as marked. (a) Model as described in section 2 and (b) modified model with less extended dumbbells.

n_3 in equation (4) separately. The functions $n_i(D)$ are all monotonic because of the cumulative effect of the event points. Consequently, plots of $n_i(D)$ do not always indicate clearly that some structural change is taking place. It can therefore be advantageous to examine the derivatives $n_i'(D) = \mathrm{d}n_i(D)/\mathrm{d}D$ of the different contributions. These give the 'density' of each type of topological event with increasing length scale D, thereby highlighting changes in the topology.

As an example, figure 4(a) shows $n_i'(D)$ for the dipolar dumbbell model at $\phi = 0.0745$ and two different temperatures. The more organised structure at lower temperature is reflected in the peaks that emerge in the solid curves. For small diameters D there is a close connection between the EC derivatives and the radial distribution function $g(r)$, which is plotted in figure 4(b) for comparison. The first peak in $g(r)$ corresponds roughly to the first peak in n_2', which dominates the full Euler characteristic $\kappa(D)$ at this stage. The correspondence arises because there is always a two-particle event halfway between any particle and its closest neighbour. Even subsequent peaks can sometimes be related, but this requires an unobstructed path between particles at such distances. An example of this correspondence is observed in the dipolar dumbbell gel at 'square' junctions, where four chains of dumbbells meet at a roughly coplanar set of four dumbbells. The distance between opposite corners of these squares is about $1.35\sigma_{\mathrm{db}}$. The joining of opposite corners is picked up in $n_2'(D)$ (because of the new contact) and $n_3'(D)$

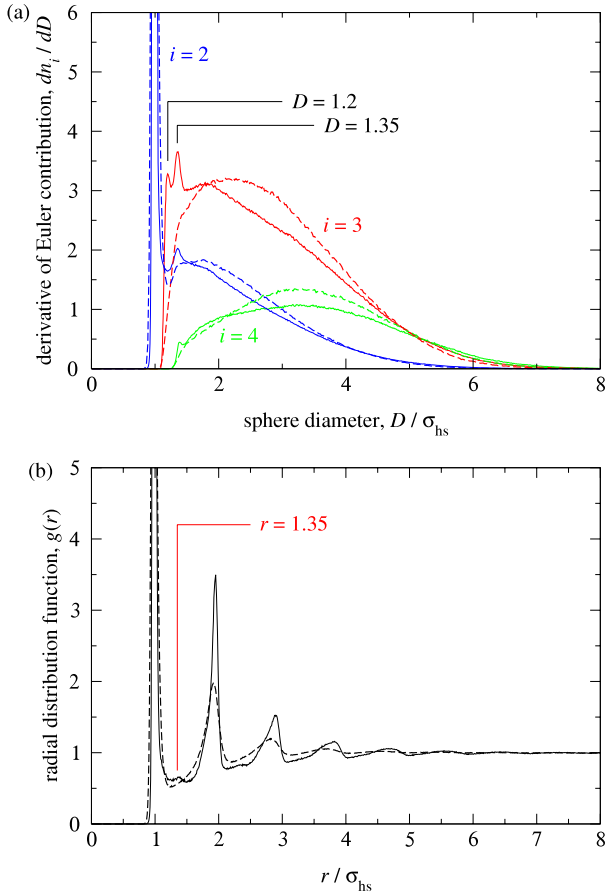

Figure 4. (a) Derivatives $n_i' = \mathrm{d}n_i/\mathrm{d}D$ of the i-particle ($i = 2, 3, 4$) topological contributions to the Euler characteristic and (b) radial distribution function for dipolar dumbbells at packing fraction $\phi = 0.0745$ and reduced temperatures $T^* = 0.041$ (solid lines) and $T^* = 0.122$ (dashed lines).

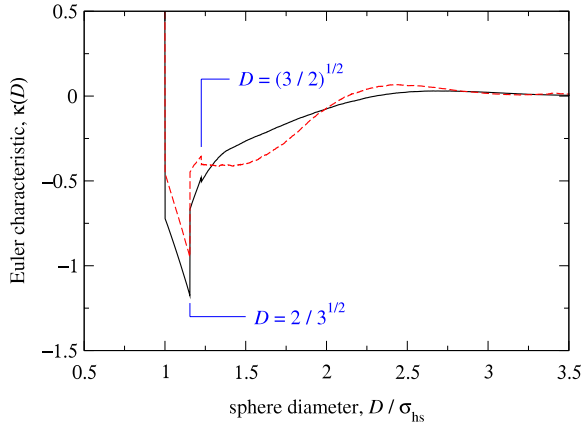

Figure 5. Euler characteristic profiles for isotropic (solid line) and patchy (dashed line) adhesive hard spheres at packing fraction $\phi = 0.262$ and effective temperature $\tau' = 0.125$.

(because a loop closes). It can also be seen as a subsidiary peak in $g(r)$.

The $n_3'(D)$ curve also clearly shows a peak around $D = 1.2\sigma_{db}$, corresponding to closure of small tori of the type illustrated in the top panels of figure 2. This peak has no partner in $n_2'(D)$ or $g(r)$, since it does not correspond to an interparticle distance. The direct connection between peaks in $g(r)$ and $\kappa'(D)$ is also lost for larger D, since the radial distribution is a two-particle correlation function, whereas the EC picks up three- and four-particle correlations and only correlates neighbouring particles via the events in which handles and holes in the surface Φ are closed. Comparison of figures 4(a) and (b) shows that topological changes continue to arise in considerable numbers at distances where the radial distribution function has virtually settled down to unity.

The connection between local structure [22] and topology can be seen clearly even in the *total* EC for the AHS fluids because of the hard repulsive core and δ-function adhesion, which lead to discontinuous changes in $\kappa(D)$. An example is shown in figure 5 at a combination of packing fraction and effective temperature that is in the percolating regime for both the isotropic and patchy cases. Discontinuities are seen at (i) $D/\sigma_{hs} = 1$, where two-particle events occur between all pairs of adhered spheres, (ii) $D/\sigma_{hs} = 2/3^{1/2}$, where tori at the centres of three mutually adhered spheres close via three-particle events (see the top panels of figure 2) and (iii) $D/\sigma_{hs} = (3/2)^{1/2}$, where holes at the centres of tetrahedra of four mutually adhered spheres close via four-particle events. The isotropic and patchy AHS profiles also differ at longer length scales. The three contributions n_2, n_3 and n_4 (not shown) all reach somewhat higher values at large D in the patchy case, indicating a greater number of topological events across a wide range of length scales. Furthermore, the contributions are all shifted to larger D, indicating that larger loops and cavities exist in the patchy case. In particular, the late approach of the EC to zero from above in the patchy case is due to the closure of large cavities in the fluid. These features suggest a more inhomogeneous structure in the fluid of patchy spheres. The adhesion leads to locally dense regions, but the patchiness prevents dense clusters from growing in all directions.

4. Percolation

As we have seen, if we consider the family of surfaces for which the Euler characteristic is determined, we find unconnected components for small sphere sizes and, on increasing the diameter, that the spheres merge and eventually percolate. Since the EC is sensitive to topological changes one might expect it to provide information on the percolation threshold. Although a completely general connection is still missing, there is some evidence that supports this idea, suggesting that the first zero of the EC forms a good estimate for the percolation threshold [23, 24].

In their work, Neher *et al* [24] examined a variety of two- and three-dimensional lattices, where each lattice point is randomly coloured black with a probability p and the remainder are white. For small values of p, some isolated black clusters are found. On increasing the value of p, the number and size of black clusters increase, and for a critical value $p = p_c$ they form a percolating structure. The nature of these lattices and the independent probability of sites being white or black enable the EC to be computed in a simple and direct way,

based on the fact that the contribution of a lattice point can be determined locally. It turns out that for the Archimedean lattices in two dimensions the first zero, at $p = p_0$, in the EC $\chi(p)$ is a close upper bound to the percolation threshold. For a selected set of lattices in three dimensions $\chi(p) = 0$ also provides a reasonable estimate of the percolation threshold.

For non-lattice models such an analysis in general is much more complicated. One exception is a random collection of equally sized penetrable spheres (an ideal gas), for which the EC per particle can still be found analytically. Using the same normalization as in the preceding section, it is given by

$$\kappa(\phi) = \left[1 - 3\phi + \frac{3\pi^2}{32}\phi^2\right]e^{-\phi}, \qquad (5)$$

where $\phi = \pi D^3\rho/6$ is the volume fraction. This is a special case of a more general result from integral geometry for clusters formed by convex grains of arbitrary shape [23]. The solution of $\kappa(\phi) = 0$ found here at $\phi_0 = 0.377$ should be compared to the percolation threshold at $\phi_c = 0.34$.

We will now test whether this apparent correlation between the zero of the EC and the percolation threshold extends to the more complex systems that we have considered. We have already seen in figure 3(b) that $\kappa(D)$ turns abruptly at a point close to $\kappa = 0$ in a system of contracted dipolar dumbbells due to the formation of well-defined unbranched chains. It should be noted, however, that the link between κ and the percolation threshold has not been proved rigorously in the general case and has only been illustrated for random, i.e. noninteracting, systems. It is therefore not clear *a priori* that such a relationship should hold for the network-forming fluids discussed in this paper.

For the dipolar dumbbell model described in section 2, we regard two dumbbells to be connected if two interaction sites—one on each particle—approach more closely than σ_{db}. To be compatible with this definition, we will need to evaluate the EC for the $2N$ interaction sites in the system of N dumbbells, rather than for the N centres-of-mass as used in figures 3 and 4. The quantity of interest with respect to the percolation threshold is then $\kappa(\sigma_{db})$, the EC evaluated at the neighbour criterion.

Figure 6(a) shows how $\kappa(\sigma_{db})$ varies with packing fraction along several isotherms. Superimposed on the isotherms is the percolation threshold as a parametric function of the reduced temperature. The percolation threshold has been defined here as the density at which 50% of the snapshots during a dynamical trajectory contain a cluster that is connected to its own images through the periodic boundary conditions. This 50% criterion is close to the crossing point in a full finite-size scaling analysis [6]. At low temperatures, the EC approaches zero at the percolation threshold, and although it becomes slightly positive as the threshold is traced to higher temperatures, it remains quite small (less than 0.04) over the wide range of packing fractions ϕ studied here. This trend can be rationalized in terms of the chain-like structure of the fluid. At low temperature, the percolation threshold lies at very low values of ϕ and the structure of the fluid is dominated by chains. Because of the low density, branches are rare, leading to a result similar to that in figure 3(b), where a uniform

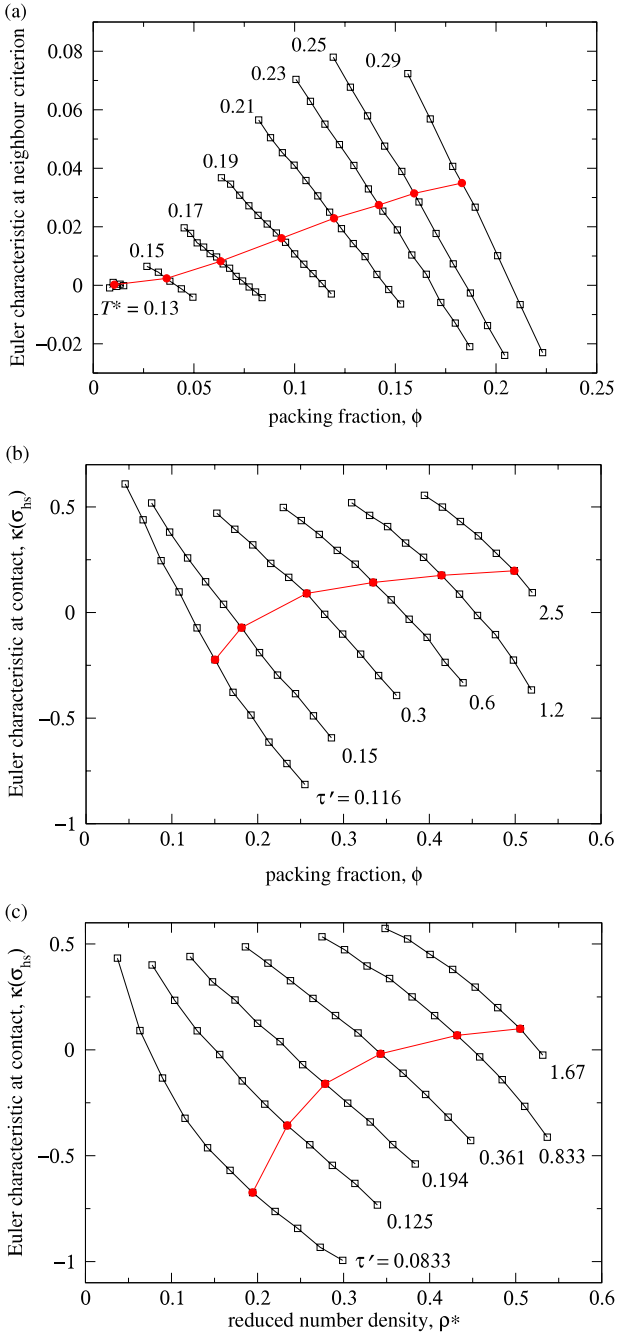

Figure 6. Open symbols: normalized Euler characteristic evaluated at the neighbour criterion along isotherms at the labelled reduced or effective temperatures. Filled symbols: percolation threshold. Lines are a guide to the eyes. (a) Dipolar dumbbell fluid, (b) adhesive hard spheres, (c) patchy adhesive hard spheres.

system of long chains has a zero EC. At higher temperatures, the percolation threshold comes at higher packing fractions, where the structure is not so dominated by clearly discernible chains. This leads to a more complicated topology, and hence a somewhat non-zero EC at contact.

Moving to more dense fluids, figures 6(b) and (c) show corresponding plots for isotropic and patchy adhesive hard spheres, respectively. Here, neighbours are unambiguously defined as pairs of spheres lying exactly σ_{hs} apart. The

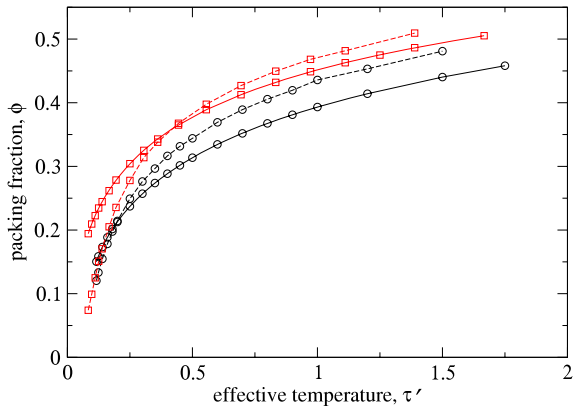

Figure 7. Percolation threshold (solid lines) and first zero of the Euler characteristic (dashed lines) for isotropic adhesive hard spheres (circles) and patchy adhesive hard spheres (squares).

isotherms of $\kappa(\sigma_{\rm hs})$ are quite steep, showing the sensitivity of the EC to density as well as to effective temperature. In the isotropic case (figure 6(b)), the percolation threshold traces out a fairly flat curve in the κ–ϕ plane at sufficiently high temperatures. However, its value is significantly non-zero (around 0.2) and there is stronger temperature dependence at lower τ'.

In the patchy case (figure 6(c)), the lack of correspondence between the percolation threshold and the zero of the EC is even more pronounced, with $\kappa(\sigma_{\rm db})$ reaching large negative values at percolation when τ' is low. This again reflects the disruption of the network by the anisotropic adhesion, leading to a structurally inhomogeneous fluid.

An alternative comparison between the EC and percolation threshold of the AHS models [17, 19] is presented in figure 7, where the zero of the EC and the percolation threshold are plotted in the τ'–ϕ plane. Percolation is suppressed by the patchiness, so that the patchy AHS threshold lies systematically at higher densities than the isotropic one. Although the $\kappa(\sigma_{\rm hs}) = 0$ curves have a qualitatively similar shape, they deviate from the percolation threshold, overestimating the percolation density at high temperature and underestimating it at low temperature.

5. Summary and concluding remarks

Being a topological invariant of a surface, the Euler characteristic is not affected by deformations that do not change the number of objects, handles and holes. Hence, for a given diameter D, the surface of overlapping spheres centred at the sites of particles in a fluid or gel gives information about the connectivity of the structure on the corresponding length scale. This information is different from and complementary to more common structural measures such as the radial distribution function, though we have seen that $\kappa(D)$ and $g(r)$ are related at short length scales. Since the EC probes connectivity on all length scales, it is most likely to be a useful tool when a system has an inhomogeneous structure, such as in low-density gels, where locally dense branches and junctions are separated by large voids.

The profile of the EC with increasing D can be rationalized in terms of the three types of topological event and the characteristic length scales on which they occur. The derivatives of the contributions, which give the density of events with respect to length scale, highlight changes in topology. A key advantage of the EC is that it responds sensitively to changes in topology that are not so easily discerned in purely structural functions. Hence, although a plot of $\kappa(D)$ does not provide an immediately intuitive picture of a system's structure, changes in $\kappa(D)$ with respect to temperature and density or to the interparticle potential, give insight into the system's response to these parameters. The EC profile itself can be regarded as a 'topological fingerprint' of the fluid. The comparisons made here between a low-density gel of dipolar dumbbells and more dense fluids of adhesive hard spheres indicate that the EC fingerprint is more informative in the former case, where a network structure and an associated topology are readily discernible.

The relationship between the percolation threshold and the first zero of the EC has been shown to depend quite strongly on the system in our selection of models. The fact that the correspondence is best for fluids dominated by chains is easily explained by the twofold coordination of particles under those conditions. Indeed, a mean coordination number of about 2 at the percolation threshold has long been investigated as a potential invariant, though significant deviations from this value are often found [25, 26]. We believe that the present contribution is the first time that the relationship between the Euler characteristic and percolation has been numerically investigated in off-lattice, strongly interacting models.

Acknowledgments

The authors thank Craig N Lumb for preparing figure 2. MAM is grateful to EPSRC (UK) for financial support.

Appendix. Calculation of the Euler characteristic

In order to compute the Euler characteristic of the family of surfaces formed by N equally sized spheres, the various event points need to be located. To this end, a Voronoi construction is first made for the set of sphere centres, because for this particular set of surfaces the event points are always located on the boundaries of the Voronoi cells.

For each face in the Voronoi construction that is intersected by the line connecting the two adjacent particle positions, a two-particle event is found. Each Voronoi edge that intersects the polygon defined by the adjacent particles contains a three-particle event. Finally, each Voronoi vertex that falls within the polyhedron formed by the adjacent particles is the location of a four-particle event. Note that in most cases the polygon and polyhedron are formed by only three and four particles, respectively. The radius of the sphere for which the event takes place is simply the distance from the event point to any of the adjacent particles.

In a simulation of a periodic system, each event should only be counted once, which can be achieved by restricting the analysis to event points that are found in the central simulation

box. The Euler characteristic can also be computed for finite samples. This relies on the fact that the computation can also be performed locally, i.e. the Voronoi cell of a single particle can be constructed and its contributions to the EC analysed. However, since event points belong to several particles, each event should be assigned a weight that is equal to the reciprocal of the number of particles adjacent to the event point. This weighting compensates for the multiple counting that arises from considering all the event points associated with each particle in turn. Following this procedure for all particles in the central box of a periodic system will lead to the same result.

For a finite sample, e.g. as obtained by confocal microscopy of colloidal particles, one typically only observes the particles within a cuboidal sub-volume of the full sample. A Voronoi construction can still be made in such a case. The Voronoi cells of the particles near the boundary of the observation window, however, will partially lie outside the range for which particles are detected and may even extend to infinity. Obviously, some of the event points calculated in this case will be wrong, because particles outside the observation window, whose positions are not known, would modify the shape of the Voronoi cells of particles within the window. In fact, even Voronoi cells that are completely situated within the observation window might not be correct. To obtain a correct EC per particle in a finite sample, only those particles should be considered for which the Voronoi cell cannot be influenced by any unobserved particle outside the viewing window. This is guaranteed when the Voronoi cell lies completely within the observation window *and* the closest distance from any point on the cell to the boundary of the observation window exceeds the distance to the particle contained in the cell. Note that, since not all particles that give rise to an event might satisfy this constraint, events that are found near the border of the sample might have a lower weight than events in the centre of the sample. This discrepancy should average out provided that the sub-volume is representative of the whole system.

References

[1] Zaccarelli E 2007 *J. Phys.: Condens. Matter* **19** 323101
[2] Bianchi E, Largo J, Tartaglia P, Zaccarelli E and Sciortino F 2006 *Phys. Rev. Lett.* **97** 168301
[3] Bianchi E, Tartaglia P, Zaccarelli E and Sciortino F 2008 *J. Chem. Phys.* **128** 144504
[4] Del Gado E and Kob W 2008 *J. Non-Newton. Fluid Mech.* **149** 28
[5] Blaak R, Miller M A and Hansen J-P 2007 *Europhys. Lett.* **78** 26002
[6] Miller M A, Blaak R, Lumb C N and Hansen J-P 2009 *J. Chem. Phys.* **130** 114507
[7] Weis J J and Levesque D 1993 *Phys. Rev. Lett.* **71** 2729
[8] Ganzenmüller G and Camp P J 2007 *J. Chem. Phys.* **126** 191104
[9] Lindahl E, Hess B and van der Spoel D 2001 *J. Mol. Modeling* **7** 306 www.gromacs.org
[10] Berendsen H J C, Postma J P M, van Gunsteren W F, DiNola A and Haak J R 1984 *J. Chem. Phys.* **81** 3684
[11] Frenkel D and Smit B 2002 *Understanding Molecular Simulation* 2nd edn (San Diego: Academic)
[12] Braun H and Hentschke R 2009 *Phys. Rev.* E **80** 041501
[13] Baxter R J 1968 *J. Chem. Phys.* **49** 2770
[14] Seaton N A and Glandt E D 1987 *J. Chem. Phys.* **87** 1785
[15] Kranendonk W G T and Frenkel D 1988 *Mol. Phys.* **64** 403
[16] Jamnik A and Bratko D 1994 *Phys. Rev.* E **50** 1151
[17] Miller M A and Frenkel D 2004 *J. Chem. Phys.* **121** 535
[18] Kern N and Frenkel D 2003 *J. Chem. Phys.* **118** 9882
[19] Fantoni R, Gazzillo D, Giacometti A, Miller M A and Pastore G 2007 *J. Chem. Phys.* **127** 234507
[20] Hoffmann N, Ebert F, Likos C N, Löwen H and Maret G 2006 *Phys. Rev. Lett.* **97** 078301
[21] Lo Verso F, Panagiotopoulos A Z and Likos C N 2009 *Phys. Rev.* E **79** 010401(R)
[22] Miller M A and Frenkel D 2004 *J. Phys.: Condens. Matter* **16** S4901
[23] Mecke K R and Wagner H 1991 *J. Stat. Phys.* **64** 843
[24] Neher R A, Mecke K and Wagner H 2008 *J. Stat. Mech.* P01011
[25] Pike G E and Seager C H 1974 *Phys. Rev.* B **10** 1421
[26] Balberg I, Anderson C H, Alexander S and Wagner N 1984 *Phys. Rev.* B **30** 3933